Chen *et al. Microstructures* 2024;4:2024033
DOI: 10.20517/microstructures.2023.89

Microstructures

Perspective

Open Access

Check for updates

Engineering electrode microstructures for advanced lithium-ion batteries

Zhou Chen[1,2], Cheng Zhang[1,2]

[1]Australian Institute for Bioengineering and Nanotechnology, The University of Queensland, Brisbane, QLD 4072, Australia.
[2]The Centre for Advanced Imaging (CAI), The University of Queensland, Brisbane, QLD 4072, Australia.

Correspondence to: Dr. Cheng Zhang, Australian Institute for Bioengineering and Nanotechnology, The University of Queensland, Build 75, Corner College Road and Cooper Road, Brisbane, QLD 4072, Australia. E-mail: c.zhang3@uq.edu.au

How to cite this article: Chen Z, Zhang C. Engineering electrode microstructures for advanced lithium-ion batteries. *Microstructures* 2024;4:2024033. https://dx.doi.org/10.20517/microstructures.2023.89

Received: 12 Dec 2023 **First Decision:** 23 Jan 2024 **Revised:** 16 Feb 2024 **Accepted:** 28 Mar 2024 **Published:** 30 May 2024

Academic Editors: Dongliang Chao, Jianfeng Mao **Copy Editor:** Fangyuan Liu **Production Editor:** Fangyuan Liu

Abstract

The architecture of anode materials is an essential factor in improving the performance of energy storage devices, which meets the increasing demand for energy storage and helps achieve environmental sustainability targets. Atomic manufacturing allows the makeup of electrodes to be changed precisely at the atomic level. This facilitates the creation of electrode materials with specific physical properties and enhanced performance. This Perspective reviews the details of how the microstructure design influences key electrode material characteristics. Finally, we anticipate the potential of materials and manufacturing techniques for materials microstructure in the future. A thorough grasp of the materials microstructure in electrode materials is offered by this article.

Keywords: Morphology, microstructures, high-performance, batteries

INTRODUCTION

For the optimal function of modern human society, energy storage technology must be reliable, cost-effective, and secure. Rechargeable lithium-ion batteries (LIBs) are the industry standard for energy storage in the rapidly growing sector of electric devices, grid storage, and portable gadgets. The current cost of LIBs is around US$150 per kilowatt-hour ($kWh^{-1}$), with a downward trend. According to the US Department of Energy, LIBs will be more economical than internal combustion engine vehicles once the cost falls below approximately US$100 kWh^{-1}[1,2]. Because of this, it is anticipated that sales of electric vehicles, which already

surpass one million units annually, will expand dramatically to over thirty million units annually by 2030. As the world increasingly relies on intermittent yet alternative energy, such as solar and wind, the grid energy storage business is expected to expand rapidly during the next decade. Consequently, it is predicted that the global demand for LIBs would increase to 1,200~1,600 GWh by 2030, exceeding ten times the demand of 2020.

While LIBs stand out as the leading rechargeable battery technology, there is still a significant difference between LIBs and gasoline in terms of energy and power density[3]. Therefore, there is a compelling need for further advancements in LIB performance. The active electrode substance composition and microstructure significantly affect energy and power density of LIBs due to their effect on the electrode production process[4-8]. Consequently, battery engineers must consider selecting and deploying active electrode materials with the desired microstructure during the battery design.

For batteries, a microstructured electrode contains active material particles within a well-structured domain with a minimum dimension of 1 μm. Microtechnology advancements have significantly enhanced the efficacy of microstructured electrodes over the last two decades. These electrodes provide advantages in power density, high-rate capability, gravimetric capacity, memory effect reduction, fracture toughness, and durability against fatigue. Furthermore, functionalizing a battery material concerning its superior rate capability, extended cycling performance and high specific capacity for LIBs has been the focus of morphology engineering[9-16]. Using synergistic benefits of each structure design, incorporating active materials into functionalized microstructural morphology can help develop novel electrochemical performance-governing materials[17-19]. While substantial research in recent decades has evaluated various nanostructured anode materials for LIBs employing distinct lithium storage, there remains a need for a comprehensive review and discussion on the intricate microengineering methodologies[20-22].

This Perspective concentrates on the discussion of developing specific morphological features, including (a) low-dimensional microstructures; (b) 3D hierarchical structures; and (c) distinctive hollow structures. These themes have gained prominence due to their unique characteristics and the significant advantages they offer in the realm of battery technology. What makes these themes so prevalent? Low-dimensional microstructures, in general, retain larger, more electrochemically active surface areas with smaller diameters. This characteristic facilitates improved contact between the electrode and the electrolyte and shorter diffusion distances. The lowest dimensional patterns that may effectively transport Li^+ and electrons are represented by 3D hierarchical porous microstructures. The advantages of micron-sized assemblies - often distinguished by a high tap density and thermodynamic stability - combine with those of nano-sized blocks in unique hollow structures.

LOW-DIMENSIONAL MICROSTRUCTURES

Extensive research has been devoted to nanomaterials as electrode materials for many years due to their numerous advantageous properties, including a substantial contact region between the electrode's surface and electrolyte, a short distance for electron and ion transport, and in some instances, the capability to conduct electrochemical reactions that are impracticable with bulk materials. Furthermore, the remarkable characteristics of the microstructure of materials can be modified by manipulating their morphologies. This enables the distinction between different microstructures based on their dimensional characteristic. According to their intrinsic dimensionality, micromaterials may be grouped according to their morphologies or intrinsic holistic form. To illustrate, (i) nanospheres are classified as zero-dimensional (0D) materials since their dimensions are exclusively at the nanoscale; (ii) anisotropic nanowires, nanorods, or nanotubes are one-dimensional (1D) materials that possess at least one dimension beyond the nanometer

range; and (iii) single or few layers of atoms or molecules make up two-dimensional (2D) materials. The layers are joined by strong covalent or ionic bonds and bound by weak van der Waals interactions.

0D nanomaterials

In contrast to bulk materials, 0D nanoparticles offer several benefits for lithium battery applications, including enhanced interfacial interaction with electrolytes, mitigation of inherent alterations in volume resulting from cyclic processes, and accelerated Li^+ transport[23]. Zhu *et al.* recently reported on applying 0D nanomaterials to enable innovative lithium battery chemistries[24]. The synthesis of spherical 5-nm lithium oxide (Li_2O) incorporated in a sub-10-nm tricobalt tetraoxide (Co_3O_4) matrix [Figure 1A] used as a cathode material in a lithium-ion battery was accomplished via a straightforward sintering procedure. By forming a condensed phase of metastable lithium peroxide (LiO_2) and lithium re-insertion, this nanocomposite enabled lithium extraction and reformation of Li_2O. For Li_2O to be stabilized by interfacial precipitation over the Co_3O_4 substrate surface, the nanoconfinement of Li_2O within the Co_3O_4 nano porous skeleton is crucial. By utilizing a confined, entirely condensed-phase configuration, this system circumvented many challenges in lithium-air batteries. The device exhibited excellent performance, as shown in Table 1.

In addition to being effective at storing lithium, 0D nanomaterials can also enhance battery performance via additional mechanisms[25]. By utilizing their polar characteristics and electronic conductivity, nanospheres of niobium carbide (NbC) were fabricated [Figure 1B] and coated on a separator to trap polysulfide (PS) intermediates. The utilization of 0D NbC for effective PS trapping, coupled with the intrinsic electronic conductivity of NbC, led to a substantial enhancement compared to the conventional configuration. Specifically, the capacity loss rate was reduced from 0.497% to 0.24%.

Despite possessing numerous electrochemical benefits compared to bulk materials, some 0D materials, including ZnO, remain intrinsically non-conductive and have restricted electronic conductivity. Carbon coating is a common way to mitigate this concern[26]. Kim *et al.* investigated carbon-coated 0D nanomaterials early[27]. Carbon was deposited onto these nanoparticles via chemical vapor deposition. The structure exhibited the most favorable characteristics: carbon-coated 10-nm Si particles demonstrated superior performance, retaining initial coulombic efficiency of 89% and 96% of their first cycle capacity after 40 cycles at 0.2 C.

Nanoparticles remain susceptible to aggregation and readily detach in intense fragmentation. A commonly utilized approach to tackle this challenge involves incorporating 0D nanomaterials onto or within carbon structures. The extended 2D structure of graphene, which provides electronic conductivity, stability, and support against pulverization during cycling, renders it an especially appealing material for loading nanoparticles. Graphene-encapsulated nickel sulfide (NiS) nanoparticles with a consistent tetrahedral structure were synthesized by AbdelHamid *et al.* in an organic solvent via a colloidal method [Figure 1C][28]. Utilizing graphene sheets to encase 25-nm particles as the anode of a lithium-ion battery resulted in an exceptionally high capacity of 542 mAh g^{-1} at 1 A g^{-1}.

1D nanomaterials

The merits of this category of nanostructures render them appealing for various LIB applications. Charge movement along the lengthwise direction is facilitated by their elongated dimension along one axis. Their advantageous stress distribution in the high aspect ratio shape helps avoid pulverization during riding. Furthermore, they are particularly advantageous for forming flexible membranes and are simple to cultivate on current collectors[29-33].

Table 1. Various morphologies of nanomaterials in energy storage, their electrochemical performance, and the importance of controlling morphology

Type	Electrode material	Function	Application	Performance	Advantages	Ref.
0D	nanocomposite Li_2O and Co_3O_4 (NC)	Cathode	LTO/NC	• Initial discharge capacity: 502 Ah kg^{-1}, then increased to 587 Ah kg^{-1} in a few cycles • Discharge capacity loss: 4.9% after 200 cycles	• Zero-dimensional morphology stabilized the synthesis of LiO_2, suppressing the growth of O_2 • Hermetically sealed condensed-phase apparatus	[24]
0D	nanocrystalline NbC	Membrane	Li-S	• Discharge capacity loss: 0.037% $cycle^{-1}$ over 1,500 cycles • C-rate: 840 and 730 mAh g^{-1} at 2 and 5 C	• The conductive NbC interlayer functions as a protective barrier, confining polysulfides. This confinement serves the dual purpose of preventing passivation of the lithium anode and mitigating self-discharge tendencies in the battery • Furthermore, the interlayer assumes the role of a "second current collector", facilitating the reutilization of trapped active materials and substantially augmenting sulfur utilization in the battery system	[25]
0D	Graphene-wrapped nickel sulfide nano prisms	Anode	Li-ion	• C-rate: 834, 656, 542, 278 and 141 mAh g^{-1} at 0.07, 0.5, 1, 3 and 5 A g^{-1}	• Increased specific area of surface and pore size facilitated enhanced electrolyte penetration within the electrochemically active region • A conductive network was created by encircling graphene	[28]
1D	Phosphorus-rich copper phosphide nanowires	Anode	Li-ion	• Initial discharge capacity and coulombic efficiency: 865 mAh g^{-1} and 57% (0.1 C) • Discharge capacity loss: 0.12% per cycle • C-rate: 1,000 and 600 mAh g^{-1} at 0.2 and 6 C (87% retention)	• The CuP_2 nanowires were designed to withstand volume expansion, resulting in increased capacity retention and decreased electrode resistance • Creating easy lithium diffusion pathways results in reduced diffusion resistance, likely linked to the development of the Li-ion conductive structure Li_3P	[34]
1D	Germanium nanowire	Anode	Li-ion	• Initial discharge capacity and coulombic efficiency: 1,103 mAh g^{-1} and 97% (0.5 C) • Discharge capacity loss: 888 mAh g^{-1} after 1,100 cycles • C-rate: 1,250, 1,174, 1,050, 821, 722, and back to 1,188 mAh g^{-1} at 0.01, 0.2, 0.5, 1, 2, and 0.01 C	• A porous network of interconnected Ge nanowires is mechanically robust to the capacity retention of the electrode.	[35]
1D	Well-aligned $Li_{0.33}La_{0.557}TiO_3$ nanowires	electrolyte	Solid battery	• Total ionic conductivity: 6.05×10^{-5} S cm^{-1} at 30 °C • Surface ionic conductivity: 1.26×10^{-2} S cm^{-1} at 30 °C	• Nanowire surfaces provide a fast ion conduction pathway without crossing junctions.	[37]
2D	Single-crystalline $LiFePO_4$ nanosheets	cathode	Li-ion	• C-rate (2D type): 151, 140, 120, 85, 72 mAh g^{-1} at 0.5, 1 5, 10, and 20 C • C-rate (bulk type): 147, 135, 85, 58, 40 mAh g^{-1} at 0.5, 1 5, 10, and 20 C • Discharge capacity loss: no obvious fading after 1,000 cycles at 10 C	• 2D nanosheets considerably enhance lithium-ion insertion/extraction efficiency, thus leading to an enhanced rate capability.	[44]
2D	Graphene-wrapped porous silicon	Anode	Li-ion	• Discharge capacity loss: 1,299.6 mAh g^{-1} after 25 cycles at 0.05 C • C-rate: 1,467.5, 1,210.6, 970.7, 697.8, and back to 1,096.8 mAh g^{-1} at 0.05, 0.1, 0.2, 0.5, and 0.05 C	• 2D morphology stabilized structure • Graphene maintained stability and conductivity	[50]
3D	Mesoporous crystalline $MoSe_2$	Anode	Li-ion	• Discharge capacity loss: 630 mAh g^{-1} after 35 cycles	• The structural stability of the 3D mesoporous $MoSe_2$ electrode leads to stable cycling performance	[53]

				• C-rate: 646, 604, 593, 557, 499, and 372 mAh g^{-1} at 0.05, 0.1, 0.2, 0.5, 1, and 2 C	• The element "Se" plays a vital role in achieving enhanced rate performance and better kinetics	
3D	Melamine-based porous organic frameworks	Cathode	Li-S	• Discharge capacity loss: 0.0508% $cycle^{-1}$ over 500 cycles • C-rate: 1,382, 1,255, 1,134, 996, 875, and 737 mAh g^{-1} at 0.1, 0.2, 0.3, 0.5, 1, and 2 C	• Melamine-based porous organic frameworks have a porous structure with very high nitrogen content and customizable porosity	[55]
3D	Urchin-like MnO/C microspheres	Anode	Li-ion	• Initial discharge capacity: 845 mAh g^{-1} • Discharge capacity loss: 723mAh g^{-1} after 80 cycles • C-rate (u-MnO): 1,157.1, 478.4, 270.5, and 81.7 mAh g^{-1} at 0.1, 0.2, 0.5, and 1 mA cm^{-2} • C-rate (u-MnO/c): from 1,197.1 to 268.3 mAh g^{-1} at 0.1, 0.2, 0.5, and 1 mA cm^{-2}	• A particular carbon film on u-MnO may buffer volume expansion during cycling • A needle-like carbon layer on u-MnO improves its electronic conductivity	[54]
3D	Sea urchin-like Si@MnO_2 @rGO	Anode	Li-ion	• C-rate: 1,323.87, 971.85, 701.12, 491.85 and 272.47 mAh g^{-1} at 0.1, 0.2, 0.5, 1, and 2 A g^{-1} • Initial discharge capacity: 1,378.14 mAh g^{-1} • Discharge capacity loss: 960.21 mAh g^{-1} after 150 cycles	• The construction that looks similar to a sea urchin keeps the anodes from getting excessively huge during cycling	[55]
3D	Flower-like Si@NiO/rGO composites	Anode	Li-ion	• C-rate: from 2,500 to 500 mAh g^{-1} at different current densities (0.1~2.0 A g^{-1}) • Discharge capacity loss: 1,081.34 mAh g^{-1} after 700 cycles at 1 A g^{-1}	• The highly percolated nanoflowers facilitated fast Li^+ diffusion and efficiently mitigated the volume expansion of Si NPs during cycling	[68]
Hollow Spheres	Hierarchical Fe_3O_4 hollow spheres	Anode	Li-ion	• Initial discharge capacity and coulombic efficiency (hollow sphere): 1,063 mAh g^{-1} and 66% (0.5 A g^{-1}) • Initial discharge capacity and coulombic efficiency (solid sphere): 800 mAh g^{-1} and 57% (0.5 A g^{-1}) • C-rate (hollow sphere): 992, 853, 716, and 548 mAh g^{-1} at 1, 2, 4, and 8 A g^{-1} • Discharge capacity loss (hollow sphere): 700 mAh g^{-1} without notable fading after 200 cycles at 3 A g^{-1} • Discharge capacity loss (solid sphere): 382 mAh g^{-1} without notable fading after 80 cycles at 0.5 A g^{-1}	• A multilayer hierarchical structure made up of nanosheet sections and a hollow structure provides a strong and spongy framework with an extensive electrode/electrolyte interface and a shorter Li^+ diffusion path • Architecture might more effectively handle the enormous changes in volume generated with frequent lithiation and delithiation	[71]
Hollow Spheres	Yolk-shell MoO_2 microspheres	Anode	Li-ion	• Initial discharge capacity and coulombic efficiency: 955.4 mAh g^{-1} and 66% (0.05 A g^{-1}) • Discharge capacity loss: 662 mAh g^{-1} after 50 cycles at 0.5 A g^{-1} (retention rate: 94.7%) • C-rate: 850, 714, and 450 mAh g^{-1} at 0.05, 0.5, and 2 A g^{-1}	• The space between individual nanoparticles (porous shell) acts as an effective buffer for the material's volume fluctuations • The yolk-shell structure aids the diffusion of Li^+ during intercalation and deintercalation by the electrolyte	[77]
Hollow Spheres	$NiCo_2O_4$ hollow spheres with complex interior structures	Anode	Li-ion	• Initial discharge capacity and coulombic efficiency: 928 mAh g^{-1} and 64% (0.15 A g^{-1})	• Small primary nanoparticles and holes may enhance the movement of Li^+, yielding a high capacity and outstanding rate capabilities	[87]

• C-rate: 834, 745, 662, and 533 mAh g^{-1} at 0.3, 0.6, 1, and 2 A g^{-1} • Discharge capacity loss: 706 mAh g^{-1} after 100 cycles at 0.2 A g^{-1} (retention rate: 78%)	• A three-layer core-in-double-shell interior construction may mitigate the significant volume changes that occur during repeated Li^+ insertion/extraction cycles

For instance, Li *et al.* developed a distinctive supercritical fluid-liquid-solid growth technique to fabricate copper phosphide (CuP_2) nanowires[34]. The synthesized CuP_2 nanowires exhibit a 1D characteristic, as evident from morphological observations in Figure 1D. Consistent with expectations, the CuP_2 nanowire sample that underwent calcination exhibits remarkable cycling performance and capacity. After undergoing 100 cycles at 100 mA g^{-1}, it maintained a capacity of 945 mAh g^{-1}, indicating its promise as an anode material for LIBs. Kennedy *et al.* documented the direct growth of Ge nanowires on the copper foil (see Figure 1E)[35]. The material exhibited a notable capacity of 1,103 mAh g^{-1} at 0.5 C, which was sustained for 1,100 cycles at 888 mAh g^{-1}. The exceptional durability of the battery can be attributed to the direct development of 1D nanowires, which formed a durable electrode that retained its exceptional stability despite material restructuring caused by protracted cycling.

Enhancing electronic conductivity is one of the benefits of the 1D morphology. An analogous pattern is observed with regard to ionic conductivity, whereby ions can swiftly traverse the longitudinal axis. Liu *et al.* reported $Li_{0.33}La_{0.557}TiO_3$ nanowires in the polymer[36,37]. By combining electrospinning and calcination, polycrystalline $Li_{0.33}La_{0.557}TiO_3$ nanowires (d < 140 nm) were produced. As shown in Figure 1F, an analysis was conducted to examine how the 1D structure affects the Li^+ conductivity compared to its 0D form. An investigation was conducted on how nanowire alignment affects the transit of Li^+. The research found that 0D nanoparticles increased the Li+ conductivity of the polymer tenfold. This improvement was primarily attributed to the increased concentration and mobility of Li^+ ions on the surface of the nanoparticles, where a very ionically conductive contact was formed with the polymer. Nevertheless, their potential was limited by the distinct features of 0D nanoparticles included in the composite and their tendency to cluster together. Replacing 0D morphology with 1D nanowires resulted in a fivefold improvement in ionic conductivity. The increase was only caused by the 1D morphology, which created a continuous channel for Li^+. Through nanowire alignment, interwire cross-junctions were effectively eliminated, resulting in a smooth flow of Li^+ across the interface between the nanowire and polymer.

Another intriguing characteristic that distinguishes 1D nanoparticle morphologies from others is that They are very beneficial for creating adaptable, freestanding membranes. The distinctive characteristic arises from the fibrous nature of 1D nanostructures, allowing them to be easily manipulated or integrated into flexible, durable structures that resemble fabric or foil. Lei *et al.* illustrated this phenomenon when they fabricated a flexible separator without binders using Al_2O_3 nanowires[38]. The resulting separator exhibited improved charge transfer, thermal stability, and wettability, all contributing to enhanced battery performance. Substituting Al_2O_3 nanowires for cellulose fiber separators resulted in a doubling of the capacity of a graphite/lithium-iron-phosphate (LFP) battery.

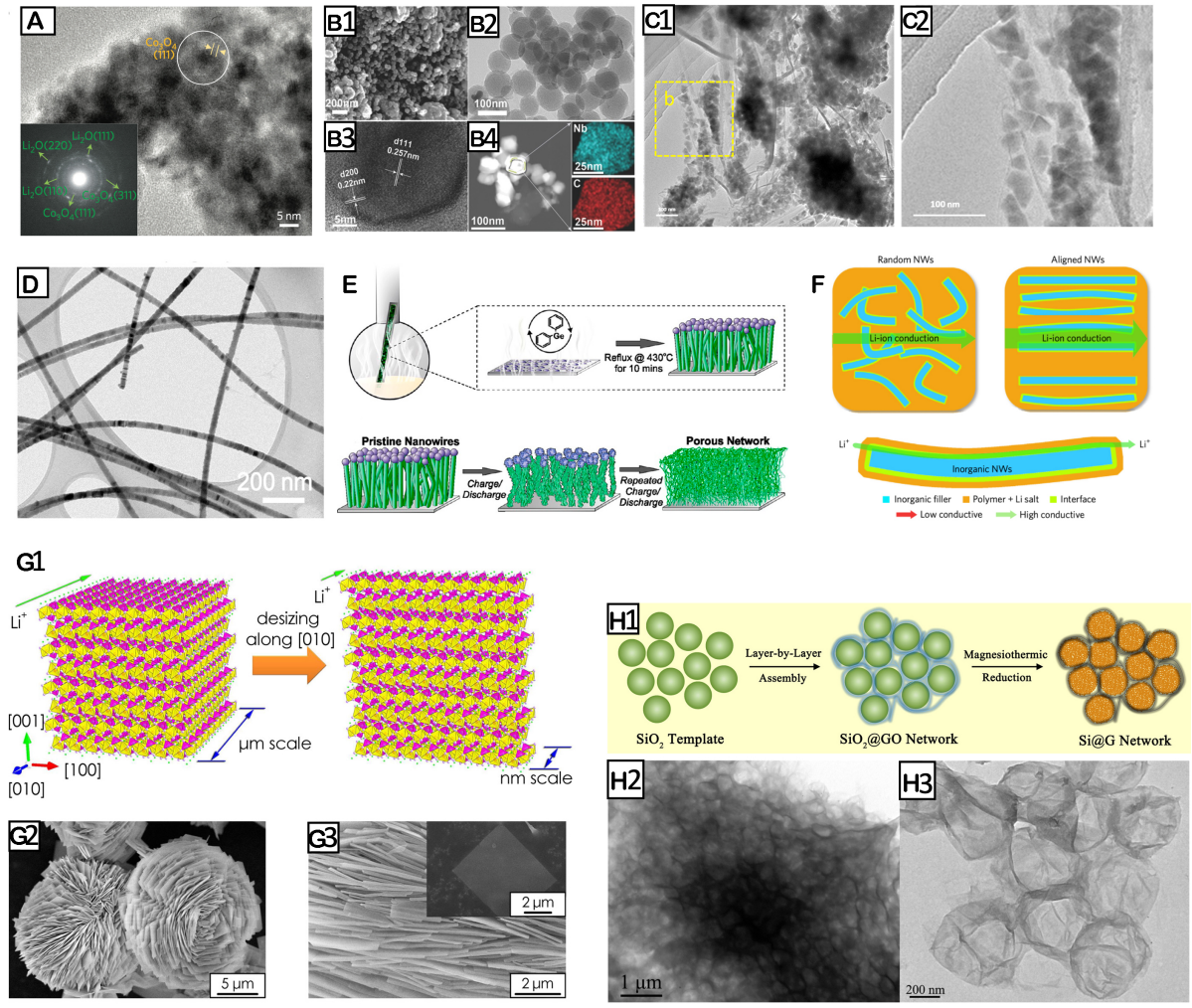

Figure 1. Illustrative examples of low-dimensional microstructure samples. (A) Transmission electron microscopy (TEM) of the nanocomposite Li_2O and Co_3O_4 powder, the circled area is a representative structure of amorphous Li_2O confined within the Co_3O_4 skeleton. Reproduced with the permission of Ref.[24] Copyright 2016, Springer Nature. (B1) SEM image, (B2) TEM image, (B3) high-resolution HRTEM image, (B4) TEM image and the elemental mapping images taken from the selected area of NbC nanospheres. Reproduced with the permission of Ref.[25] Copyright 2017, John Wiley & Sons. (C1) TEM and (C2) magnified TEM images of the boxed area in (C1) of NiS nanoparticles. Reproduced with the permission of Ref.[28] Copyright 2016, Elsevier. (D) TEM images of CuP_2 nanowires. Reproduced with the permission of Ref.[34] Copyright 2016, American Chemical Society. (E) Schematic illustrating the synthetic method used for NW growth and schematic showing the cumulative effect of cycling on the NW architecture. The pristine Ge NW array is transformed into a porous, interconnected network of active material due to the charge/discharge process. Reproduced with the permission of Ref.[35] Copyright 2014, American Chemical Society. (F) Aligned ceramic $Li0.33La0.557TiO3$ nanowires for hybrid solid electrolyte. Li^+ conduction paths in solid polymer electrolyte containing random and aligned nanowires. Express Li^+ conduction along the ceramic/polymer interface. Reproduced with the permission of Ref.[37] Copyright 2017, Springer Nature. (G1) Crystal structure and surface energy of $LiFePO_4$ crystals and the schematic illustration of shortening the lithium-ion diffusion distance along the [010]; structural and phase purity characterization of the $LiFePO_4$ nanosheets; (G2) representative SEM image of the as-synthesized $LiFePO_4$ particles; (G3) SEM image showing the latitudinally accumulated nanosheets. Inset: an individual nanosheet obtained after exfoliation. Reproduced with the permission of Ref.[44] Copyright 2014, American Chemical Society. (H1) Schematic illustration for the synthesis of the Si@G network. (H2 and H3) TEM images of the 3D interconnected graphene network at different magnifications. Reproduced with the permission of Ref.[50] Copyright 2014, American Chemical Society.

2D nanomaterials

The preferential exposure of specific facets in the 2D structures plays a pivotal role in facilitating rapid ion and electron transfer, thereby enhancing the efficiency of lithium storage. In addition, the mechanical flexibility of 2D nanomaterials is enhanced by their ultrathin thickness, making them ideal for creating

elastic, thin, and flexible LIBs[39,40]. The substantial area-to-volume ratio of the nano-thin materials enables excellent contact with the electrolyte and promotes in-plane electron and ion transport. Additionally, the prolonged lateral dimensions establish uninterrupted ion transport pathways. Furthermore, the impact of stress-strain cycles during battery operation is mitigated by the 2D nanostructures, thereby improving overall battery stability[41,42]. Electrode materials exhibiting anisotropic Li^+ diffusion could benefit significantly from implementing 2D nanomaterials. The 2D morphology of these materials was intentionally structured to restrict the diffusion of Li^+ along the 2D plane, substantially improving both the rate capability and diffusion velocity of Li^+. Concurrently, in contrast to the 0D morphology, sizable 2D sheets exhibit greater volumetric energy density and stability due to their reduced side reactions with the electrolyte.

An investigation comparing the LFP with different carbon materials revealed that 2D graphene nanosheets disperse more evenly in the electrode matrix than carbon nanotubes (CNT) and acetylene black (AB)[43]. The LFP-graphene composite in the study demonstrated a diffusion coefficient of 5.9×10^{-9} cm^2/s and an interface resistance value of around 130 Ω cm^{-2}. The figures were around 150%-300% greater than those of the CNT and AB. This pertains to the development of extended electron routes and the elevated electron conductivity shown by this category of 2D materials. Zhao *et al.* produced LFP nanosheets that are single-crystalline and have a thickness ranging from 30 to 60 nm in the [010] direction [Figure 1G][44]. The nanosheets also have micrometric lateral dimensions. The synthesis process controlled the morphology and crystal structure, with diethylene glycol stabilizing the planes throughout the solvothermal reaction. This stabilization was achieved due to the interaction energy, effectively inhibiting growth in the [010] orientation. Consequently, the surface coverage of the [010] plane exceeded 93%, significantly improving Li^+ by tenfold compared to traditional LFP powder. This improvement further resulted in a 50% reduction in polarization and an increased capability to operate at high rates. Specifically, a capacity of 90 mAh g^{-1} was reached at a rate of 10 C, and the stability over 1,000 cycles was found to be extremely excellent. This method limited the nanoscale size in the best direction for Li^+ diffusion while maintaining a micrometer size in the other directions. Consequently, it improved the transit of Li^+, decreased surface area, and minimized negative interactions with the electrolyte.

The remarkable mechanical properties of a network created by 2D materials around the electrode particles can prevent fracturing and improve the stability of the electrochemical reaction. Typically, an amount of weight between 10% and 60% of the mass of active materials is utilized to improve the mechanical strength and electrochemical efficiency of electrodes[45-49]. Wu *et al.* investigated the pulverization of silicon nanoparticles that occurs throughout the cycling process[50]. They achieved this by creating a hybrid nanostructure consisting of graphene-wrapped silicon/carbon nanofibers (Si/CNF-G). Figure 1H shows the conceptual design, transmission electron microscopy (TEM) image of the Si/CNF-G nanosheet composite and the corresponding cycle performance at different silicon ratios. The electrode without a binder showed a reversible capacity of 878 mA h g^{-1} over 100 cycles for the optimized sample. However, the silicon electrode could only sustain a reversible discharge capacity of 200 mA h g^{-1} after 100 cycles.

3D HIERARCHICAL STRUCTURES

Hierarchical structures offer significant benefits in the field of LIBs. Firstly, using nanosized building blocks ensures short distances for both electronic and Li^+ transport, enhancing electrochemical activity. Secondly, the porous nature of these nanostructures facilitates effective impregnation of electrolytes and ensures a suitable region of contact, thereby improving rate performance. Lastly, the ordered structure of these nanostructures allows them to endure the stress from lithium insertion or extraction, therefore prolonging the battery cycle life[51].

Mesoporous structures

Typically, hierarchical nanostructures formed by nanoparticles consist of numerous fundamental building blocks with diameters falling within the range of tens of nanometers. This results in the creation of a porous framework with a fairly large surface area[52]. Shi *et al.* developed a nanocoating method using mesoporous silica SBA-15 as a stiff template to manufacture well-organized mesoporous crystallized MoSe2[53]. The MoSe2 particles created have a rod-like shape and structured mesostructure formed from the SBA-15 precursors [Figure 2A]. The mesoporous $MoSe_2$ sample exhibits distinctive structural characteristics, resulting in a discharge capacity of 630 mAh g^{-1} after 35 cycles. This capacity significantly surpasses its predicted capacity achieved by the four-electron conversion process.

Porous organic polymers (POPs) may provide an alternative porous structure. Given the extensive range of different types of persistent organic pollutants, the capabilities and applications of POPs are likewise very diverse and include several sectors, particularly in batteries based on lithium chemistry. The use of POPs for immobilizing active substances has mostly been limited to the domain of Li-S batteries[54,55]. As shown in Figure 2B, the performance of Li-S batteries is influenced by the well-documented PS shuttle effect, which arises from the solubility of intermediate reaction products known as PSs. POPs have primarily been utilized in two manners: (1) by chemisorbing intermediate PS species to hinder their dissolution and diffusion out of the cathode; and (2) by forming covalent bonds between sulfur and insoluble POPs, thereby preventing PS dissolution during discharge (the covalent bonds between sulfur and the POP host are ideally maintained during lithiation/delithiation).

POPs produced by porous carbon exhibit a high number of active sites and improved conductivity, enabling quick and reversible lithium-ion intercalation/de-intercalation. Additionally, it has enough void spaces to tolerate volume variations, facilitating rapid redox reactions. The physical characteristics such as shape, size, surface area, and the presence of different elements in the structure of porous carbon materials may significantly influence their ability to conduct electricity. Porous carbon materials have been synthesized using POPs in order to attain a substantial specific surface area, which facilitates efficient electrolyte penetration and redox processes. The presence of enriched micro and mesopores allows for rapid and effective ion transport and enhances the accessibility to the active surface. Furthermore, the simple modification of POPs allows for the inclusion of diverse heteroatoms inside their molecular framework. Lithium ions in the electrolyte are propelled towards lithium-affinitive sites on the negative electrode surface by combining electric potential gradients, lithium-ion concentration gradients, and electrostatic interactions with electronegative sites within the electrode framework. Doping atoms should establish electronegative sites (doping atoms or adjacent carbon atoms) as Lewis bases to interact with lithium ions acting as Lewis acids. Therefore, sites carrying a greater negative charge are believed to induce stronger interactions with lithium ions. Moreover, lithium affinity is not solely determined by acid-base interactions; it is also influenced by other factors such as the local geometric and electronic structure of the dopant. Thus, introducing the concept of local dipoles becomes necessary: doping atoms form dipoles with adjacent carbon atoms, thereby further enhancing the binding energy. These factors collectively contribute to the enhancement of lithium storage capacity. Subsequently, these heteroatoms may be transformed into heteroatom-doped carbon upon exposure to high temperatures, hence enhancing the capacity for lithium-ion storage[56-58].

Urchin-like nanospheres

The urchin-like hierarchical structures, formed by assembling 1D building blocks, possess structural benefits derived from both the overarching hierarchical structures and the fundamental low-dimensional components. Consequently, these complex formations exhibit improved lifespan and quicker response kinetics[39,59].

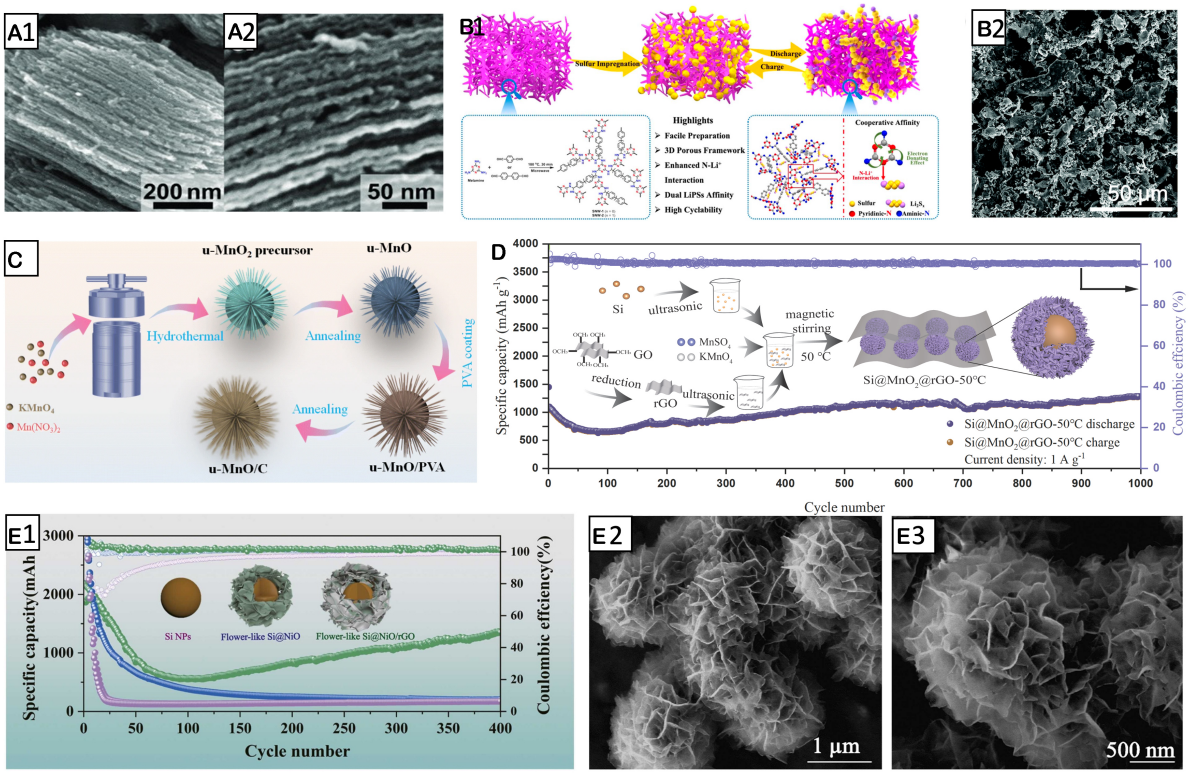

Figure 2. Illustration of the preparation, morphology and performance of 3D hierarchical nanostructures. (A1 and A2) SEM images of the synthesized mesoporous $MoSe_2$ materials using SBA-15 as the template via nanocoating method. Reproduced with the permission of Ref.[53] Copyright 2012, John Wiley & Sons. (B) Synthetic schematic of SNW/S and working mechanism of LiPSs trapping. Reproduced with the permission of Ref.[55] Copyright 2021, IOPScience. (C) Schematic illustration for the preparation process of u-MnO and u-MnO/C. Reproduced with the permission of Ref.[62] Copyright 2021, Springer Nature. (D) Concise preparation schematics of the Si@MnO_2@reduced graphene oxide (rGO) composites and long-term cycling performance of the Si@MnO_2@rGO-50 °C at 1 A g^{-1}. Reproduced with the permission of Ref.[63] Copyright 2022, MDPI Journals. (E1) SEM image of Si@NiO; (E2) Enlarged SEM image of Si@NiO composite. (E3) Schematic diagram of the preparation of Si@NiO/rGO composite and long-term cycling performance of Si, Si@NiO, and Si@NiO/rGO at 0.1 A g^{-1}. Reproduced with the permission of Ref.[68] Copyright 2023, Elsevier.

The Urchin-like materials have a spherical shape composed of nanorods, with a hollow macroporous core. To achieve this category, the gradual decomposition of functional ligands plays a pivotal role in the genesis of intricate hierarchical nanostructures[60]. This core may function as an electrolyte reservoir, and the nanorods facilitate rapid diffusion of the electrolyte and effectively accommodate the strain generated during cycling[61]. Zhang *et al.* manufactured urchin-like MnO/C microspheres by a hydrothermal technique and thermal degradation of polyvinyl alcohol (PVA) on the MnO surface [Figure 2C][62]. The electrochemical performance for lithium storage is enhanced in u-MnO/C due to its distinctive hierarchical nanostructures and carbon coatings. The u-MnO/C anode has a notable initial discharge capacity of 845 mAh g^{-1}. After 80 cycles, the discharge capacity may be maintained at 723 mAh g^{-1}. The discharge capacity of u-MnO is just 397 mAh g^{-1}.

Liu *et al.* recommended a straightforward hydrothermal technique to synthesize sea urchin-like Si@MnO_2@reduced graphene oxide(rGO) structures for use as anodes[63]. The combination of MnO_2 and rGO encapsulating Si nanospheres creates a robust protective layer that mitigates the mechanical stress caused by expanding Si nanospheres. Additionally, this protective layer creates sufficient buffer space, contributing to an extended lifespan. The Si@MnO_2@rGO anode, shaped akin to a sea urchin, showed an initial discharge capacity of 1,378.15 mAh g^{-1} at a current density of 0.1 A g^{-1}. After over 1,000 cycles, the

discharge-specific capacity was 1,282.72 mAh g^{-1} at a current density of 1 A g^{-1} [Figure 2D]. This demonstrates the exceptional chemical performance of the anode under various current densities.

Flower-like nanostructures

Flower-shaped structures have gotten numerous attention among various forms inspired by nature. This is attributed to their notably larger surface area than circular particles, leading to more effective interactions at the surface[64]. The morphology and dimensions of artificially fabricated flower-like structures may be manipulated to regulate both the stability of the structure and the performance of surface activities[65].

The flower-shaped configuration enhances the contact area of electrodes, increases the wetting properties of electrolytes, and expedites the movement of lithium ions, improving rate performance[66,67]. Furthermore, these self-supported electrodes can eliminate the need for additional binders or conductive additives, enhancing the specific capacity even further[30]. Pan *et al.* produced a Si@NiO/rGO anode with a distinctive flower-like structure[68]. This was achieved using a straightforward and effective one-step synthesis process to encapsulate Si inside the flower-like NiO structure [Figure 2E1 and E2] while evenly embedding rGO nanosheets in the "petals" of NiO. Figure 2E3 displays the rate performance of these anodes at different current densities ranging from 0.1 to 2.0 A g^{-1}. The performance of all three anodes decreases with increasing current density from 0.1 to 2 A g^{-1}. Si@NiO/rGO composite had superior capacity maintenance than Si@NiO and Si/rGO, despite all recovering and remaining stable when current density returns to 0.1 A g^{-1}. The Si@NiO/rGO hybrid maintains a capacity maintenance rate of about 77.08% with a reversible capacity of 1,794.22 mAh g^{-1}. The unique layout of silicon nanoparticles encased in nickel oxide nanoflowers and rGO nanosheets within the nickel oxide “petal” structure makes for excellent performance. This construction allows quick electrolyte penetration and lithium-ion diffusion and improves silicon nanoparticle swelling buffer zones.

DISTINCTIVE HOLLOW STRUCTURES

Hollow structures are particularly valuable as hosts for active electrode materials, offering a functionality exclusive to morphologies with dimensions of 0D and 2D. Additionally, 1D nanostructures can include active substances within their empty core. However, the small volume of nanotubes makes it challenging to load a significant quantity of active substances. Therefore, 3D hollow nanostructures are well-documented and very effective for this particular purpose. Various hollow 3D structures, including single-shell and multi-level architectures, have been created to meet the growth in volume of anode materials in LIBs, offering both physical and chemical confinement that enables greater storage of Li^+.

Single-shell architecture

Hollow structures are built with a single layer of active material around an interior void. The synthesis techniques for these structures typically employ either template-engaged or template-free procedures[69,70]. Ma *et al.* created hollow balls using extremely thin Fe_3O_4 nanosheets[71]. The self-engaged template consists of solid spheres containing a precursor of iron, which is composed of Fe-ions and isopropyl alcohol, referred to as Fe-IPA. During the solvothermal process, Fe-IPA spheres gradually change to hierarchical Fe-glycerate hollow spheres made up of sheet-like subunits. Following a further annealing process, the resulting Fe_3O_4 hollow spheres maintained the initial monocoque design of the Fe-glycerate precursors without any evident damage to structures [Figure 3A]. The single-shelled Fe_3O_4 void spheres possess exceptional structural stability due to their extremely porous structure and sheet-like subunits, enabling them to endure volume changes throughout repeated cycles. Consequently, these empty spheres provide an unnoticeable decrease after 100 cycles.

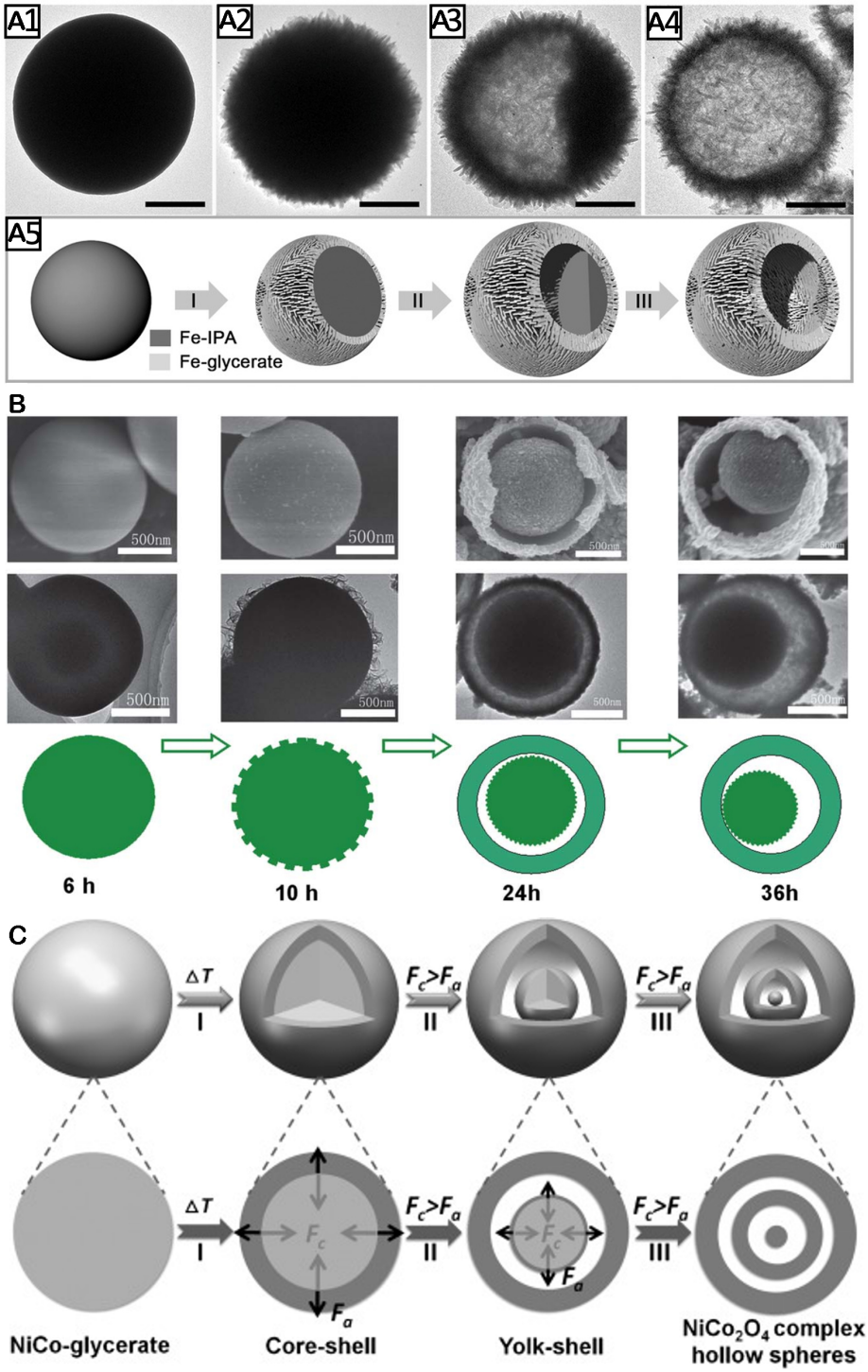

Figure 3. Structural information of distinctive hollow structures. TEM images of the Fe-IPA with hollow structure obtained after reaction for (A1) 1 h, (A2) 2 h, (A3) 4 h, and (A4) 12 h. The scale bars are 300 nm; (A5) Schematic illustration of the formation process of Fe-glycerate hollow spheres: (I) formation of Fe-glycerate nanosheets on the surface of the initially formed Fe-IPA solid spheres; (II) further growth of Fe-glycerate nanosheets and consumption of Fe-IPA spheres; (III) formation of hierarchical Fe-glycerate hollow spheres. Reproduced with the permission of Ref.[71] Copyright 2015, John Wiley & Sons. (B) Schematic illustration of the formation process of yolk-shell MoO_2 microspheres. Reproduced with the permission of Ref.[77] Copyright 2013, Royal Society of Chemistry. (C) Schematic illustration of the formation process of $NiCo_2O_4$ core-in-double-shell hollow spheres. Reproduced with the permission of Ref.[87] Copyright 2014, John Wiley & Sons.

Multi-level architecture

The advantages of single-shelled hollow constructions are offset by the excess vacant space, which greatly reduces the tapping density of the active materials, resulting in low volumetric power and energy density[52,69]. Hollow nanostructures with multi-level architecture, such as those with yolk-shells and multi-shells, have been suggested to avoid these problems[72-79]. By optimizing the use of the interior cavity of hollow structures, these intricate designs successfully raise the weight fraction of the electrochemically active components[52]. Furthermore, the structural stability might be further improved using the multi-level design as physical supports[80]. In addition, the electrolyte might penetrate the inner area via the void spaces of these hollow structures, which could also handle the volume fluctuations that occur during repeated charging and discharging cycles.

The yolk-shell architecture is a distinct kind of core-shell structure defined by a certain core-void-shell arrangement[78,81,82]. Metal oxides with a yolk-shell structure are being closely studied as potential electrode materials in LIBs because they can prevent the clumping of active nanoparticles inside them and handle the substantial volume changes occurring throughout cycling. Yolk-shell structured SnO_2, Co_3O_4, V_2O_5, and Fe_2O_3 have been claimed to provide improved cycling capabilities[83-86]. Zhang *et al.* produced yolk-shell monodisperse MoO_2 microspheres devoid of a template [Figure 3B][77]. The yolk-shell MoO_2 microspheres have exceptional electrochemical performance, which is of great significance. At a current density of 50 mAh g^{-1}, these batteries may provide a substantial charge of 955 mAh g^{-1} during the first discharge. Moreover, they may retain a reversible capacity of 847.5 mAh g^{-1} after 50 cycles.

Multi-shelled micro-/nano hollow structures with more than two shells are expected to have superior properties than single-shell structures because of their larger area of surface, lower density, and improved loading capacity. Hollow constructions with many shells may be readily created using hollow shells as templates. Due to the permeable nature of the template's shell, the chosen shell material will coat both the inner and outer surfaces of the templates, forming uninterrupted layers of coating. Shen *et al.* proposed a novel and effective approach to produce homogenous $NiCo_2O_4$ hollow spheres with intricate internal architecture[87]. This method first entails synthesizing NiCo-glycerate solid spheres using a straightforward solvothermal technique. Subsequently, the solid spheres of NiCo-glycerate may be transformed into complicated hollow spheres of $NiCo_2O_4$ by a straightforward process of heat annealing in the presence of air [Figure 3C]. The complicated internal structure that forms during the thermal disintegration of metal glycerate is a consequence of the combined influence of contraction and adhesion activities resulting from non-equilibrium heat treatment. This technology has been shown to have the potential to be used widely for synthesizing metal oxide complex hollow spheres. The $NiCo_2O_4$ hollow spheres have a distinctive inner structure consisting of a core surrounded by two concentric shells. The porous shells comprise tiny nanocrystalline particles. After 100 cycles of continuous cycling at a current density of 200 mAh g^{-1}, the battery retains a reversible discharge capacity of 706 mAh g^{-1}, equivalent to 78% of the discharge capacity seen in the second cycle. More precisely, the existence of minute primary nanoparticles and holes might enhance the movement of Li^+ ions, leading to a greater storage capacity and exceptional ability to charge and discharge quickly. Significantly, the distinctive three-layer core-in-double-shell interior structure can absorb the substantial volume change that occurs during the repeated insertion and extraction of Li^+ ions during cycling. This structure also provides structural integrity, thereby reducing the problem of pulverization and improving the stability of the cycling process.

One essential factor for electrode materials is the mechanical property, particularly concerning the calendering process employed during optimized electrode film production. This approach focuses on tightly packing electrode materials to improve the electrical connection between the active material and conductive ingredients and enhance adhesion between the active material and foil. The calendering process involves

substantial pressure, reaching up to 80 MPa. Under such conditions, numerous nanostructures could fall apart, potentially limiting the practical application of these structures. Fortunately, composition, crystallinity, nano subunit aggregation, shell thickness, and shell number may be controlled to make hollow structures resistant to high pressure. For instance, an amorphous carbon shell is brittle and prone to cracking with minimal deformation, while a graphene cage exhibits mechanical strength and flexibility, displaying exceptional resistance to pressure from the exterior[88]. Moreover, metal oxides typically demonstrate better mechanical robustness than carbon materials. Experimental results from *in situ* TEM indentation show that a TiO_2 hollow sphere containing a 16 nm shell thickness remains structurally intact at a pressure of 160 MPa, while an amorphous carbon hollow sphere disintegrates at pressures below 41 MPa[89]. While numerous well-designed hollow nano- and microstructures have been documented, the challenge persists in devising controlled, reproducible methods to produce materials with precise composition and specific geometric attributes in high-quality hollow nano- and microstructures, meeting the requirements of practical applications. Consequently, there is a pressing need for increased endeavors in the synthesis-controlled development of electrode materials.

Lastly, it is imperative to underscore that the hollow structure may not universally benefit electrode materials[90]. Specifically, when employed as electrode materials, hollow structured materials often exhibit comparatively lower Coulombic efficiency and tap density. The critical consideration lies in judiciously applying the appropriate structure in a context-specific manner, thereby maximizing the advantages of hollow materials in mitigating volumetric deformation and ion dissolution. While the hollow structure proves advantageous, it is not omnipotent.

CONCLUSION

In summary, each of these discussed morphologies has distinct advantages that make them particularly well-suited for use in LIBs. Various nanoparticle shapes are used to store electricity according to unique material needs (refer to Table 1). Nanostructures have similar characteristics such as large surface areas and fast Li^+ transport dynamics, but each morphological category has distinct qualities ideal for certain applications. The basic 0D structure was first used in energy storage, demonstrating the promise of nanotechnology in progressing this subject. However, a recent trend involves transitioning to higher-order morphologies to mitigate drawbacks associated with 0D nanoparticles, such as electrolyte side reactions, interparticle contact resistance, and aggregation tendencies. Nevertheless, 0D nanoparticles remain optimal for certain applications, particularly in designs involving nano-confined active materials and situations where the maximization of catalytic and adsorption properties is crucial. Moreover, the effectiveness of these nanoparticles is notable when incorporated into higher-order morphologies, resulting in hybrid structures that exhibit synergistic performance while mitigating the drawbacks associated with 0D configurations. La Mer's mechanism primarily considers the size homogeneity of nanoparticles by temporally separating the nucleation stage from the growth process. However, a universal theory to elucidate the uniformity in nanoparticle morphology is currently lacking, which requires future studies.

The 1D materials present many appealing characteristics, including high aspect ratios, reduced lattice boundaries, which is the interface between two grains, or crystallites, in a polycrystalline material but seldom found in 1D materials, and a restricted presence of harmful flaws, making them appealing as electrode materials. Notably, the easy convertibility of 1D shape into cloth-like membranes holds great promise for applications in separators and flexible electronics. The 1D structure may have a hollow core, which improves mass dispersion and exposure of catalytic sites. This makes it useful as an active material host in Li-O_2 and Li-S battery systems.

The 2D topology allows for unlimited charge transport in two planar directions while constraining just the in-plane dimension. This enhances structural stability, minimizes side reactions, and preserves favorable nanostructured attributes, notably rapid kinetics. To achieve an ideal design, it is important to restrict the flow direction perpendicular to Li^+ diffusion pathways in order to enhance the Li^+ transit efficiency. The flat 2D shape is beneficial for catalytic purposes in Li-O_2 batteries and may be used as a base for attaching 0D nanoparticles to form advanced composite nanomaterials. However, the dearth of scientific factors elucidating the heightened mechanical flexibility of 2D nanomaterials remains conspicuous. Diverse methodologies have been deployed to investigate the mechanical behaviors of 2D materials across varied conditions. Predominantly, mechanical assessments rely on the nanoscale indentation technique of atomic force microscopy, characterized by a markedly uneven stress distribution concentrated at the contact point of the indenter. Interestingly, this method is infrequently applied in battery research. Therefore, the exigency for quantitative scientific metrics is pronounced to systematically analyze the mechanical flexibility of 2D nanomaterials in the context of battery research, providing valuable insights into the influence of material thickness on their performance.

The 3D nanostructures provide several intrinsic and crucial benefits for energy storage compared to electrodes composed solely of 0D nanoparticles or 1D nanowires of electroactive materials. Firstly, they have a significantly large active surface area crucial for enhancing the accessibility of lithium ions and improving electrochemical reactions between metal oxide materials and the electrolyte. Secondly, these motifs feature an adjustable overall free volume that accommodates the expansion of metal oxides during lithium insertion. Lastly, they contribute to reduced Li^+ diffusion distances, resulting in shorter transport lengths for the movement of Li^+ in both intercalation materials and conversion or alloying reactions. In order to enhance the utilization of nanostructures with varying shapes in lithium rechargeable batteries, it is crucial to focus specifically on the following aspects.

DISCUSSION AND PERSPECTIVES

Future investigations on hollow micro-/nanostructures should prioritize examining both fundamental and practical elements. It is crucial to comprehend current synthetic processes to create more dependable and scalable approaches for generating void micro-/nanostructures in an economical and environmentally friendly way. Improved insight into the underlying mechanisms may facilitate the generalization of these approaches, paving the way for their applications in industrial settings. Additionally, it can enable the design and production of materials with intricate structures and desired qualities that were previously unattainable. The extensive development of synthetic techniques will allow the use of such hollow frameworks as adaptable basic units that can be readily included in developing and manufacturing novel practical substances and technologies.

Defective electrode materials, encompassing heteroatom doping, inherent defects, vacancy defects, and other structural modifications, are highly desirable in advanced batteries. As a result, these defects can enhance ion diffusion and electron transfer. Introducing defects into nanomaterials has two main benefits. Firstly, it expands the storage capacity for foreign ions, improving battery capacity. Secondly, these defects act as effective adsorption sites, particularly for intermediates, preventing undesirable shuttle effects.

Anode-free lithium batteries are an advanced technology that has the potential to outperform the current gradual improvements in lithium battery lifespan. They offer a remarkable increase of up to 60% in energy density. In an anode-free lithium battery, a naked copper foil is used as the anode, allowing lithium to migrate from the cathode and deposit onto the copper current collector during the first formation cycle. However, challenges arise from high consumption of Li^+ in an unstable solid electrolyte interphase (SEI)

and dendrite formation, resulting in significant instability. Nanomaterials with precisely regulated shapes at both the nano and macroscales have significant promise for addressing this issue. Various strategies with regulated structure and permeability have been shown to effectively control and redistribute the flow of Li^+, hence reducing the production of dendrites and stabilizing the SEI. This research path involves using creative structural design and suitable material composition to achieve significant breakthroughs in anode-free technology.

The extensive library of nanomaterial production technologies facilitates the creation of hybrid nanomaterials, composed of multiple components, each uniquely tailored for particular purposes. This method allows for the development of versatile nanostructures, particularly useful for intricate cells such as Li-S[91-93] and solid batteries[94-96], in which various components can conduct distinct tasks within the same system. Examples include sulfur storing, PS capture, transformation, and conductivity improvement. To improve battery performance, integrating emerging technologies, such as artificial intelligence, will undoubtedly aid in designing novel nanomaterials and nanocomposites and their combination with organic substances such as binders and additives. The synergistic benefits of these advancements make further developments of this technology highly promising for lithium rechargeable batteries.

The design of electrode structure is a pivotal determinant of battery performance, necessitating considering multiple factors for optimization. Key considerations in this area include: (1) Surface Area and Porosity: Enhancing electrode surface area through micro- or nano-architectures with well-defined porosity facilitates efficient electrolyte interaction, augmenting ion transport and thereby improving battery capacity; (2) Particle Dimensions and Morphology: Optimal sizing and shaping of electrode particles influence the rate of electron and ion transport, with nanostructures particularly effective in reducing electron pathways and enhancing battery performance; and (3) Conductivity and Pathway Optimization: Ensuring high conductivity by including conductive materials or additives is imperative for efficient electron transport within the electrode structure. These design principles, contingent on battery type and application, form the basis for achieving enhanced battery performance and reliability.

Two main issues hinder the effective deployment of nanotechnology for LIBs. One primary factor is the intricate and expensive techniques used in producing nanomaterials, particularly those with intricate structures. The second reason is the use of non-commercial criteria for evaluating novel nanostructures, including minimal bulk loading, surplus electrolyte, and low electrode density. Despite these challenges, alloy-based anode nanomaterials have shown significant advancements in commercial applications after a decade of extensive research and refinement. Initiatives in expansion and automobile production are expected to integrate industrial perspectives into developing lithium rechargeable batteries, considering factors such as practicality, cost, and adherence to industry testing requirements.

DECLARATIONS

Authors' contributions

Drafted the manuscript: Chen Z
Participated in the writing, revision and literature discussion: Chen Z, Zhang C
Finalized the manuscript: Chen Z, Zhang C

Conflict of interest

Both authors declared that there are no conflicts of interest.

Availability of data and materials

Not applicable.

Financial support and sponsorship

This work is supported by the Australian Research Council (LP220100036) and the University of Queensland Knowledge Exchange & Translation Grants for funding. Zhang C acknowledges the Australian Research Council for his Discovery Early Career Researcher Award fellowship (DE230101105).

Ethical approval and consent to participate

Not applicable.

Consent for publication

Not applicable.

REFERENCES

1. Nykvist B, Nilsson M. Rapidly falling costs of battery packs for electric vehicles. *Nat Clim Change* 2015;5:329-32. DOI
2. Ziegler MS, Trancik JE. Re-examining rates of lithium-ion battery technology improvement and cost decline. *Energy Environ Sci* 2021;14:1635-51. DOI
3. Hundekar P, Jain R, Lakhnot AS, Koratkar N. Recent advances in the mitigation of dendrites in lithium-metal batteries. *J Appl Phys* 2020;128:010903. DOI
4. Ellis BL, Lee KT, Nazar LF. Positive electrode materials for Li-ion and Li-batteries. *Chem Mater* 2010;22:691-714. DOI
5. Lotfabad EM, Ding J, Cui K, et al. High-density sodium and lithium ion battery anodes from banana peels. *ACS Nano* 2014;8:7115-29. DOI
6. Liu C, Li F, Ma LP, Cheng HM. Advanced materials for energy storage. *Adv Mater* 2010;22:E28-62. DOI
7. Naguib M, Halim J, Lu J, et al. New two-dimensional niobium and vanadium carbides as promising materials for Li-ion batteries. *J Am Chem Soc* 2013;135:15966-9. DOI
8. Wang Q, Huang Y, Miao J, Zhao Y, Wang Y. Synthesis and electrochemical characterizations of Ce doped SnS_2 anode materials for rechargeable lithium ion batteries. *Electrochim Acta* 2013;93:120-30. DOI
9. Fu X, Zhou Y, Huang J, et al. Rethinking the electrode multiscale microstructures: a review on structuring strategies toward battery manufacturing genome. *Adv Energy Mater* 2023;13:2301385. DOI
10. Lu X, Zhang X, Tan C, et al. Multi-length scale microstructural design of lithium-ion battery electrodes for improved discharge rate performance. *Energy Environ Sci* 2021;14:5929-46. DOI
11. Lee HJ, Liu X, Chart Y, et al. $LiNi_{0.5}Mn_{1.5}O_4$ cathode microstructure for all-solid-state batteries. *Nano Lett* 2022;22:7477-83. DOI PubMed PMC
12. Li J, Liang X, Liou F, Park J. Macro-/micro-controlled 3D lithium-ion batteries via additive manufacturing and electric field processing. *Sci Rep* 2018;8:1846. DOI PubMed PMC
13. Feng Z, Peng W, Wang Z, et al. Review of silicon-based alloys for lithium-ion battery anodes. *Int J Miner Metall Mater* 2021;28:1549-64. DOI
14. Vernardou D. Recent report on the hydrothermal growth of $LiFePO_4$ as a cathode material. *Coatings* 2022;12:1543. DOI
15. Wang X, Zhang C, Sawczyk M, et al. Ultra-stable all-solid-state sodium metal batteries enabled by perfluoropolyether-based electrolytes. *Nat Mater* 2022;21:1057-65. DOI
16. Wang Y, Wu Z, Azad FM, et al. Fluorination in advanced battery design. *Nat Rev Mater* 2024;9:119-33. DOI
17. Pam ME, Yan D, Yu J, et al. Microstructural engineering of cathode materials for advanced zinc-ion aqueous batteries. *Adv Sci* 2020;8:2002722. DOI PubMed PMC
18. Lin L, Zhang L, Wang S, Kang F, Li B. Micro- and nano-structural design strategies towards polycrystalline nickel-rich layered cathode materials. *J Mater Chem A* 2023;11:7867-97. DOI
19. Reddy MV, Subba Rao GV, Chowdari BV. Metal oxides and oxysalts as anode materials for Li ion batteries. *Chem Rev* 2013;113:5364-457. DOI PubMed
20. Mahmood N, Tang T, Hou Y. Nanostructured anode materials for lithium ion batteries: progress, challenge and perspective. *Adv Energy Mater* 2016;6:1600374. DOI
21. Yuan C, Wu HB, Xie Y, Lou XW. Mixed transition-metal oxides: design, synthesis, and energy-related applications. *Angew Chem Int Ed* 2014;53:1488-504. DOI PubMed

22. Chen G, Yan L, Luo H, Guo S. Nanoscale engineering of heterostructured anode materials for boosting lithium-ion storage. *Adv Mater* 2016;28:7580-602. DOI
23. Poizot P, Laruelle S, Grugeon S, Dupont L, Tarascon JM. Nano-sized transition-metal oxides as negative-electrode materials for lithium-ion batteries. *Nature* 2000;407:496-9. DOI PubMed
24. Zhu Z, Kushima A, Yin Z, et al. Anion-redox nanolithia cathodes for Li-ion batteries. *Nat Energy* 2016;1:16111. DOI
25. Cai W, Li G, Zhang K, et al. Conductive nanocrystalline niobium carbide as high-efficiency polysulfides tamer for lithium-sulfur batteries. *Adv Funct Mater* 2018;28:1704865. DOI
26. Roland A, Fullenwarth J, Ledeuil J, Martinez H, Louvain N, Monconduit L. How carbon coating or continuous carbon pitch matrix influence the silicon electrode/electrolyte interfaces and the performance in Li-ion batteries. *Battery Energy* 2022;1:20210009. DOI
27. Kim H, Seo M, Park MH, Cho J. A critical size of silicon nano-anodes for lithium rechargeable batteries. *Angew Chem Int Ed* 2010;49:2146-9. DOI
28. Abdelhamid AA, Yang X, Yang J, Chen X, Ying JY. Graphene-wrapped nickel sulfide nanoprisms with improved performance for Li-ion battery anodes and supercapacitors. *Nano Energy* 2016;26:425-37. DOI
29. Zhu C, Usiskin RE, Yu Y, Maier J. The nanoscale circuitry of battery electrodes. *Science* 2017;358:eaao2808. DOI PubMed
30. Lu Y, Yu L, Lou XW. Nanostructured conversion-type anode materials for advanced lithium-ion batteries. *Chem* 2018;4:972-96. DOI
31. Mai L, Sheng J, Xu L, Tan S, Meng J. One-dimensional hetero-nanostructures for rechargeable batteries. *ACC Chem Res* 2018;51:950-9. DOI
32. Zhang X, Shyy W, Marie Sastry A. Numerical simulation of intercalation-induced stress in Li-ion battery electrode particles. *J Electrochem Soc* 2007;154:A910. DOI
33. Wu Y, Yao Y, Wang L, Yu Y. Recent progress on modification strategies of alloy-based anode materials for alkali-ion batteries. *Chem Res Chin Univ* 2021;37:200-9. DOI
34. Li GA, Wang CY, Chang WC, Tuan HY. Phosphorus-rich copper phosphide nanowires for field-effect transistors and lithium-ion batteries. *ACS Nano* 2016;10:8632-44. DOI PubMed
35. Kennedy T, Mullane E, Geaney H, Osiak M, O'Dwyer C, Ryan KM. High-performance germanium nanowire-based lithium-ion battery anodes extending over 1000 cycles through in situ formation of a continuous porous network. *Nano Lett* 2014;14:716-23. DOI PubMed
36. Liu W, Liu N, Sun J, et al. Ionic conductivity enhancement of polymer electrolytes with ceramic nanowire fillers. *Nano Lett* 2015;15:2740-5. DOI
37. Liu W, Lee SW, Lin D, et al. Enhancing ionic conductivity in composite polymer electrolytes with well-aligned ceramic nanowires. *Nat Energy* 2017;2:17035. DOI
38. Lei D, Benson J, Magasinski A, Berdichevsky G, Yushin G. Transformation of bulk alloys to oxide nanowires. *Science* 2017;355:267-71. DOI PubMed
39. Cong L, Xie H, Li J. Hierarchical structures based on two-dimensional nanomaterials for rechargeable lithium batteries. *Adv Energy Mater* 2017;7:1601906. DOI
40. Liu B, Zhang J, Shen G. Pursuing two-dimensional nanomaterials for flexible lithium-ion batteries. *Nano Today* 2016;11:82-97. DOI
41. Pomerantseva E, Bonaccorso F, Feng X, Cui Y, Gogotsi Y. Energy storage: the future enabled by nanomaterials. *Science* 2019;366:eaan8285. DOI PubMed
42. Rojaee R, Shahbazian-Yassar R. Two-dimensional materials to address the lithium battery challenges. *ACS Nano* 2020;14:2628-58. DOI PubMed
43. Zhao D, Feng Y, Wang Y, Xia Y. Electrochemical performance comparison of $LiFePO_4$ supported by various carbon materials. *Electrochim Acta* 2013;88:632-8. DOI
44. Zhao Y, Peng L, Liu B, Yu G. Single-crystalline $LiFePO_4$ nanosheets for high-rate Li-ion batteries. *Nano Lett* 2014;14:2849-53. DOI
45. Casimir A, Zhang H, Ogoke O, Amine JC, Lu J, Wu G. Silicon-based anodes for lithium-ion batteries: effectiveness of materials synthesis and electrode preparation. *Nano Energy* 2016;27:359-76. DOI
46. Zhou G, Wang D, Li F, et al. Graphene-wrapped Fe_3O_4 anode material with improved reversible capacity and cyclic stability for lithium ion batteries. *Chem Mater* 2010;22:5306-13. DOI
47. Li S, Wang B, Li B, Liu J, Yu M, Wu X. Self-assembly of 2D sandwich-structured $MnFe_2O_4$/graphene composites for high-performance lithium storage. *Mater Res Bull* 2015;61:369-74. DOI
48. Wang B, Li X, Zhang X, et al. Adaptable silicon-carbon nanocables sandwiched between reduced graphene oxide sheets as lithium ion battery anodes. *ACS Nano* 2013;7:1437-45. DOI
49. Agyeman DA, Song K, Lee G, Park M, Kang Y. Carbon-coated Si nanoparticles anchored between reduced graphene oxides as an extremely reversible anode material for high energy-density Li-ion battery. *Adv Energy Mater* 2016;6:1600904. DOI
50. Wu P, Wang H, Tang Y, Zhou Y, Lu T. Three-dimensional interconnected network of graphene-wrapped porous silicon spheres: in situ magnesiothermic-reduction synthesis and enhanced lithium-storage capabilities. *ACS Appl Mater Interfaces* 2014;6:3546-52. DOI
51. Zhang L, Wu HB, Lou XW. Iron-oxide-based advanced anode materials for lithium-ion batteries. *Adv Energy Mater* 2014;4:1300958. DOI
52. Yu L, Hu H, Wu HB, Lou XW. Complex hollow nanostructures: synthesis and energy-related applications. *Adv Mater* 2017;29:1604563. DOI PubMed
53. Shi Y, Hua C, Li B, et al. Highly ordered mesoporous crystalline $MoSe_2$ material with efficient visible-light-driven photocatalytic

activity and enhanced lithium storage performance. *Adv Funct Mater* 2013;23:1832-8. DOI

54. Zhao J, Yan G, Hu Z, Zhang X, Shi J, Jiang X. Triazine-based porous organic polymers with enhanced electronegativity as multifunctional separator coatings in lithium-sulfur batteries. *Nanoscale* 2021;13:12028-37. DOI
55. Sun M, Ji H, Guan Y, et al. Nanoscale melamine-based porous organic frameworks as host material for efficient polysulfides chemisorption in lithium-sulfur batteries. *Nanotechnology* 2021;32:085402. DOI
56. Je SH, Kim HJ, Kim J, Choi JW, Coskun A. Perfluoroaryl-elemental sulfur S_NAr chemistry in covalent triazine frameworks with high sulfur contents for lithium-sulfur batteries. *Adv Funct Mater* 2017;27:1703947. DOI
57. Kim J, Elabd A, Chung S, Coskun A, Choi JW. Covalent triazine frameworks incorporating charged polypyrrole channels for high-performance lithium-sulfur batteries. *Chem Mater* 2020;32:4185-93. DOI
58. Liu J, Li H, Wang J, et al. Design zwitterionic amorphous conjugated micro-/mesoporous polymer assembled nanotentacle as highly efficient sulfur electrocatalyst for lithium-sulfur batteries. *Adv Energy Mater* 2021;11:2101926. DOI
59. Trogadas P, Ramani V, Strasser P, Fuller TF, Coppens MO. Hierarchically structured nanomaterials for electrochemical energy conversion. *Angew Chem Int Ed* 2016;55:122-48. DOI PubMed
60. Fuchigami T, Yamamoto H, Tanibata N, Nakayama M, Kakimoto K. Growth mechanism of spiky Nb_2O_5 nanoparticles and their electrochemical property. *Phys Status Solidi* 2022;259:2100642. DOI
61. Xing Y, Wang S, Fang B, Song G, Wilkinson DP, Zhang S. N-doped hollow urchin-like anatase TiO_2@C composite as a novel anode for Li-ion batteries. *J Power Sources* 2018;385:10-7. DOI
62. Zhang L, Shen L, Liu Y, Suo G. Urchin-like MnO/C microspheres as high-performance lithium-ion battery anode. *Ionics* 2021;27:1423-8. DOI
63. Liu J, Wang M, Wang Q, et al. Sea urchin-like Si@MnO_2@rGO as anodes for high-performance lithium-ion batteries. *Nanomaterials* 2022;12:285. DOI PubMed PMC
64. Zou Y, Wang Y. Microwave solvothermal synthesis of flower-like SnS_2 and SnO_2 nanostructures as high-rate anodes for lithium ion batteries. *Chem Eng J* 2013;229:183-9. DOI
65. Bhosale SV, Al Kobaisi M, Jadhav RW, Jones LA. Flower-like superstructures: structural features, applications and future perspectives. *Chem Rec* 2021;21:257-83. DOI PubMed
66. Hao Q, Cui G, Zhao Y, Bakenov Z. Flower-like $MoSe_2$/MoO_2 composite with high capacity and long-term stability for lithium-ion battery. *Nanomaterials* 2019;9:1256. DOI PubMed PMC
67. Chen X, Zhang H, Yan P, Cao X, Zhan C, Liu J. Flower-like metal oxide composite as an efficient sulfur host for stable and high-capacity lithium-sulfur batteries. *J Solid State Chem* 2022;314:123430. DOI
68. Pan J, Sun C, Liu J, et al. One-step synthesis method of flower-like Si@NiO/rGO composites as high-performance anode for lithium-ion batteries. *J Alloys Compd* 2023;947:169506. DOI
69. Wang X, Feng J, Bai Y, Zhang Q, Yin Y. Synthesis, properties, and applications of hollow micro-/nanostructures. *Chem Rev* 2016;116:10983-1060. DOI
70. Wang Z, Zhou L, Lou XW. Metal oxide hollow nanostructures for lithium-ion batteries. *Adv Mater* 2012;24:1903-11. DOI PubMed
71. Ma FX, Hu H, Wu HB, et al. Formation of uniform Fe_3O_4 hollow spheres organized by ultrathin nanosheets and their excellent lithium storage properties. *Adv Mater* 2015;27:4097-101. DOI
72. Zhang G, Xia BY, Xiao C, et al. General formation of complex tubular nanostructures of metal oxides for the oxygen reduction reaction and lithium-ion batteries. *Angew Chem Int Ed* 2013;52:8643-7. DOI
73. Yu L, Guan B, Xiao W, Lou XW. Formation of yolk-shelled Ni-Co mixed oxide nanoprisms with enhanced electrochemical performance for hybrid supercapacitors and lithium ion batteries. *Adv Energy Mater* 2015;5:1500981. DOI
74. Zhang G, Lou XW. General synthesis of multi-shelled mixed metal oxide hollow spheres with superior lithium storage properties. *Angew Chem Int Ed* 2014;53:9041-4. DOI PubMed
75. Wu LL, Wang Z, Long Y, et al. Multishelled $Ni_xCo_{3-x}O_4$ hollow microspheres derived from bimetal-organic frameworks as anode materials for high-performance lithium-ion batteries. *Small* 2017;13:1604270. DOI
76. Wang J, Yang N, Tang H, et al. Accurate control of multishelled Co_3O_4 hollow microspheres as high-performance anode materials in lithium-ion batteries. *Angew Chem Int Ed* 2013;52:6417-20. DOI
77. Zhang X, Song X, Gao S, et al. Facile synthesis of yolk-shell MoO_2 microspheres with excellent electrochemical performance as a Li-ion battery anode. *J Mater Chem A* 2013;1:6858. DOI
78. Ko YN, Choi SH, Park SB, Kang YC. Preparation of yolk-shell and filled Co_9S_8 microspheres and comparison of their electrochemical properties. *Chem Asian J* 2014;9:572-6. DOI PubMed
79. Lu Y, Yu L, Wu M, Wang Y, Lou XWD. Construction of complex Co_3O_4@$Co_3V_2O_8$ hollow structures from metal-organic frameworks with enhanced lithium storage properties. *Adv Mater* 2018;30:1702875. DOI
80. Qi J, Lai X, Wang J, et al. Multi-shelled hollow micro-/nanostructures. *Chem Soc Rev* 2015;44:6749-73. DOI
81. Bruce PG, Scrosati B, Tarascon JM. Nanomaterials for rechargeable lithium batteries. *Angew Chem Int Ed* 2008;47:2930-46. DOI PubMed
82. Ma Y, Bi R, Yang M, et al. Hollow multishelled structural ZnO fillers enhance the ionic conductivity of polymer electrolyte for lithium batteries. *J Nanopart Res* 2023;25:14. DOI
83. Liu J, Zhou Y, Wang J, Pan Y, Xue D. Template-free solvothermal synthesis of yolk-shell V_2O_5 microspheres as cathode materials for Li-ion batteries. *Chem Commun* 2011;47:10380-2. DOI

84. Lou XW, Li CM, Archer LA. Designed synthesis of coaxial SnO_2@carbon hollow nanospheres for highly reversible lithium storage. *Adv Mater* 2009;21:2536-9. DOI
85. Wang X, Wu X, Guo Y, et al. Synthesis and lithium storage properties of Co_3O_4 nanosheet-assembled multishelled hollow spheres. *Adv Funct Mater* 2010;20:1680-6. DOI
86. Zhong J, Cao C, Liu Y, Li Y, Khan WS. Hollow core-shell eta-Fe_2O_3 microspheres with excellent lithium-storage and gas-sensing properties. *Chem Commun* 2010;46:3869-71. DOI
87. Shen L, Yu L, Yu XY, Zhang X, Lou XW. Self-templated formation of uniform $NiCo_2O_4$ hollow spheres with complex interior structures for lithium-ion batteries and supercapacitors. *Angew Chem Int Ed* 2015;54:1868-72. DOI PubMed
88. Li Y, Yan K, Lee H, Lu Z, Liu N, Cui Y. Growth of conformal graphene cages on micrometre-sized silicon particles as stable battery anodes. *Nat Energy* 2016;1:15029. DOI
89. Jin Y, Li S, Kushima A, et al. Self-healing SEI enables full-cell cycling of a silicon-majority anode with a coulombic efficiency exceeding 99.9%. *Energy Environ Sci* 2017;10:580-92. DOI
90. Lu S, Sun Y, Xu Y, Guo S, Cao A, Wan L. Hollow-structured electrode materials: self-templated synthesis and their potential in secondary batteries. *ChemNanoMat* 2020;6:1298-314. DOI
91. Wu H, Li Y, Ren J, et al. CNT-assembled dodecahedra core@nickel hydroxide nanosheet shell enabled sulfur cathode for high-performance lithium-sulfur batteries. *Nano Energy* 2019;55:82-92. DOI
92. Song Z, Jiang W, Jian X, Hu F. Advanced nanostructured materials for electrocatalysis in lithium-sulfur batteries. *Nanomaterials* 2022;12:4341. DOI PubMed PMC
93. Wang F, Zuo Z, Li L, He F, Li Y. Graphdiyne nanostructure for high-performance lithium-sulfur batteries. *Nano Energy* 2020;68:104307. DOI
94. Gu Y, You EM, Lin JD, et al. Resolving nanostructure and chemistry of solid-electrolyte interphase on lithium anodes by depth-sensitive plasmon-enhanced Raman spectroscopy. *Nat Commun* 2023;14:3536. DOI PubMed PMC
95. Abdelhamid AA, Mendoza-garcia A, Ying JY. Advances in and prospects of nanomaterials' morphological control for lithium rechargeable batteries. *Nano Energy* 2022;93:106860. DOI
96. Huang J, Guo X, Du X, et al. Nanostructures of solid electrolyte interphases and their consequences for microsized Sn anodes in sodium ion batteries. *Energy Environ Sci* 2019;12:1550-7. DOI